Optimization of methane cold wall chemical vapor deposition for the production of single walled carbon nanotubes and devices

P. Finnie [a,b,*], A. Li-Pook-Than [b], J. Lefebvre [a], D.G. Austing [a]

[a] *Institute for Microstructural Sciences, National Research Council Canada, Building M-50, Montreal Road, Ottawa, ON, Canada K1A OR6*
[b] *Department of Physics, University of Ottawa, 150 Louis Pasteur, Ottawa, ON, Canada K1N 6N5*

Abstract

Carbon nanotubes are synthesized by cold wall chemical vapor deposition (CVD) using methane as the carbon source and iron thin film catalyst. The yield of thin nanotubes as determined by scanning electron microscopy (SEM) is strongly dependent on the precise CVD process and the preparation of the substrate. The effects of pressure (5–80 kPa), temperature (700–950 °C), substrate conditioning (air preheat) and metallization (Fe, Al, Mo) on thin nanotube yield are reported. High yields of thin nanotubes are obtained under optimum conditions. These thin nanotubes are candidates to be single walled carbon nanotubes (SWNTs) and Raman spectroscopy, photoluminescence spectroscopy and electrical transport provide evidence that, at least at optimum conditions, many, and perhaps all of the thin nanotubes are single walled. Single nanotube field effect transistors are fabricated and factors affecting device yield are reported. Optimum single nanotube device yield does not necessarily coincide with the optimum nanotube yield.
Crown Copyright © 2006 Published by Elsevier Ltd. All rights reserved.

Keywords: Carbon nanotubes; Chemical vapor deposition; Scanning electron microscopy; Optical properties; Electrical (electronic) properties

1. Introduction

Chemical vapor deposition (CVD) is presently the leading method of synthesizing carbon nanotubes. Drawing on earlier methods of synthesizing larger filaments, the methods of single walled nanotube (SWNT) synthesis developed in the mid- to late-1990s have proliferated widely, and expanded into a family of related methods. Very generally, CVD methods can be classified into "hot wall" and "cold wall" categories [1]. In hot wall methods, a furnace, including its sidewalls is heated. In cold wall methods, only the sample itself is heated. This seemingly insignificant difference is of considerable practical importance.

The early work on SWNT CVD, and what might now be called the "standard method" of SWNT synthesis focused on hot wall methods [2]. However, cold wall methods have many advantages, including economy, and compatibility with optical monitoring. It is also a natural approach for plasma CVD methods, and therefore much of the work on multiwalled carbon nanotubes (MWNT) has been cold walled.

Previously we reported using cold wall CVD to synthesize SWNTs [3]. We found the process to be somewhat inconsistent in terms of day-to-day yield of synthesized product, and in terms of uniformity across a given sample. However, we have improved our own cold wall CVD process. Others have also successfully used cold wall methods [4]. In general, progress in the CVD synthesis of SWNTs has been rapid and all the lessons from hot wall CVD apply to cold wall CVD. Using newer substrate preparation methods, characterization methods and growth recipes, cold wall CVD appears to be just as reliable as hot wall CVD. Below we will show how process parameters, including CVD pressure, temperature, and sample preparation affect the yield of thin nanotubes as observed by SEM.

---

* Corresponding author. Address: Institute for Microstructural Sciences, National Research Council Canada, Building M-50, Montreal Road, Ottawa, ON, Canada K1A OR6. Fax: +1 613 990 0202.
E-mail address: Paul.Finnie@nrc.ca (P. Finnie).

At optimized conditions we show that many, if not all, of these thin nanotubes are SWNTs. We also fabricate single nanotube FETs and examine how these parameters affect device yield.

2. Experiments

We used a simple home-built cold wall CVD reactor (Fig. 1). The reactor was a short pyrex cylinder (diameter ~7 cm, total internal volume ~0.8 L) mated to stainless steel flanges. The sample (rectangular, total area ~1 cm^2) was clipped on a miniature hot stage, only slightly larger than the sample, and heated by thermal conduction. The hot stage was suspended on posts used to supply current for heating. Alternatively, the sample could be heated by passing a current directly through the sample. While both heating methods produced SWNTs, the hot stage provided better temperature uniformity. Therefore, all data presented here were obtained with conductive heating via the hot stage.

Gas was admitted by a ~6 mm diameter tube directed at the center of the sample at a distance of ~2 cm and an angle of ~60° from the substrate normal. As illustrated in Fig. 1b, hydrogen and methane gas injection rates were regulated by upstream mass flow controllers (FC). A turbomolecular pump (TP) was used to evacuate the chamber to its base pressure. The turbomolecular pump was then isolated by a shutoff valve (crossed circle). When gas was admitted, a scroll pump (SP) was used to maintain a fixed pressure. The pressure was measured by a Baratron gauge (P) and regulated by a needle valve (crossed circle with arrow).

All samples were derived from ~0.4 mm thick, lightly phosphorus doped (10 Ω cm) Si(1 0 0) wafers capped with 1 μm thermal SiO$_2$. The catalyst consisted of a layer of aluminum (~1 nm) with iron on top (~1 nm) deposited by electron beam evaporation. Samples were exposed to air during the interval between the deposition of aluminum and iron.

Photolithography was used to prepare four sample types (Fig. 2). For the catalyst-only samples (Fig. 2a), circular catalyst islands of ~2 μm in diameter (illustrated), as well as more elongated shapes of similar scale (not shown) were prepared by photolithography. For molybdenum contact samples (Fig. 2b), prior to catalyst deposition, molybdenum fingers were prepared by a separate lithography step, with deposition by magnetron sputtering. Fingers of various shapes were prepared, typically several microns wide, ~70 μm long, and ~200 nm thick. For chromium gold contact samples (Fig. 2c), gold fingers of similar geometry to the molybdenum fingers were patterned by lithography after CVD growth of nanotubes. For trench samples (Fig. 2d), prior to catalyst deposition the silicon dioxide was etched to form trench and hole patterns. Trenches and holes were a few microns wide, with vertical sidewalls, and etched down to the silicon, 1 μm deep.

Before CVD growth, some samples were preheated to 300 °C in air. The effect of this conditioning step will be shown below. The standard CVD process was as follows. In the first step, a reduction step, hydrogen was flown at 200 sccm until the chamber reached a pressure of 66 kPa, after which the sample was heated to a fixed temperature in the range 700 °C to 950 °C under a continuous flow of hydrogen for 10 min. Temperatures were measured with an optical pyrometer having a 2 mm diameter sampling spot centered on the substrate. Next was the growth step, in which methane was introduced to initiate the growth of SWNTs. Methane was introduced at various flow rates, with a co-flow of hydrogen maintained. Typical flow rates were 200 sccm for methane and 20 sccm of hydrogen (10:1 ratio) as measured by mass flow controllers. Typical temperatures for the growth step ranged from 700 °C to 950 °C. Methane was flown for several minutes, after which the hydrogen was ramped up to 200 sccm and the methane ramped down to no flow. Finally, hydrogen alone was flown for ~15 min, diluting the residual methane to below a partial pressure of 7 kPa as verified by a residual gas analyzer sampling the exhaust. The heating current was then shut off and the sample cooled to ~100 °C within ~1 min.

Next, we briefly explain the rationale for the main elements of the CVD process. The reduction step serves two purposes, first it helps ensure that the iron is not in the form of an oxide [5,6] and second to change the thin film catalyst morphology, producing nanoparticle catalysts. The reduction of Fe$_2$O$_3$ in a hydrogen atmosphere is spontaneous above ~425 °C, and the reduction of Fe$_3$O$_4$ is spontaneous above ~625 °C. It is believed that oxides poison the catalyst, so this would appear to set a lower bound on the temperature for which SWNTs can be grown using iron alone as the catalyst. However, it should be noted that very recent research has challenged the assumption that oxides are ineffective catalysts [7]. Of course, a further complication is that phase diagrams derived from bulk materials do not necessarily apply directly to nanoparticles so these temperatures are only approximate.

The temperature range of the growth step can be rationalized if the enthalpy and entropy of formation of SWNTs change little from that of bulk graphite. Since the decomposition of methane to form graphite and hydrogen gas is spontaneous only above ~650 °C, this is likely to represent a lower limit to the temperature for the growth of SWNTs via thermal CVD with methane as the carbon source. At high temperatures (~1000 °C) reactions of catalyst particles with the substrate can poison the growth [8].

Recent reports for CVD with ethylene [9] indicate that trace water vapor and perhaps other oxidizing trace gases can change the yield and distribution of carbon nanotubes. Here, we have used research grade purity gas, and evacuated the chamber with a turbopump before each growth run, but beyond that, we have not intentionally controlled the levels of oxidizing trace gases. It is worth pointing out that the levels of trace gases such as water vapor may be quite different for cold wall CVD as compared to hot walled CVD. Unlike Ref. [9], we did not observe forest growth, however, although similar catalyst was used, ethylene is much more unsta-

Fig. 2. Sample schematics: (a) catalyst island only sample, (b) molybdenum contact sample, (c) chromium gold contact sample and (d) trench sample.
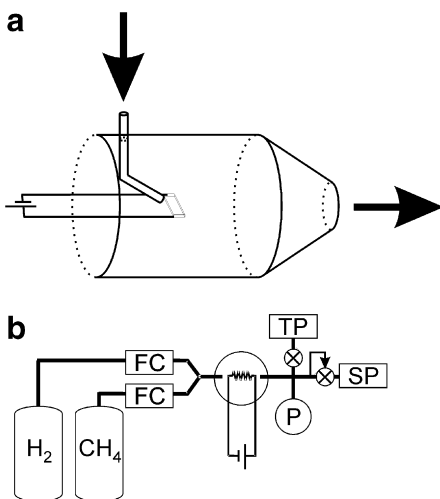
Fig. 1. Cold wall CVD schematic: (a) reactor schematic (approximately to scale) and (b) gas flow schematic. The acronyms are explained in the main text.
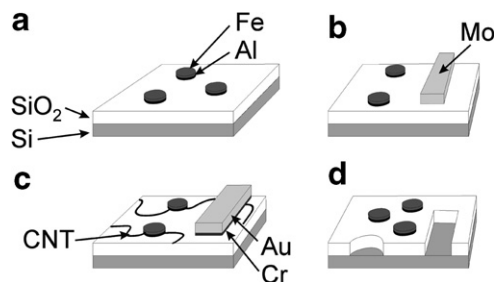
ble than methane, which should cause a higher carbon yield, but may also result in increased MWNT growth. Methane source and iron catalyst based plasma CVD methods, inherently more reactive than thermal methods, have been recently been reported to produce SWNT forests [10].

To analyze the yield all samples were examined by scanning electron microscopy (SEM), our primary characterization tool. Scanning electron microscopy is rapid and under appropriate operating conditions easily reveals even single SWNTs. In "charging mode", one does not image the nanotube itself but rather the charge that accumulates on an insulating surface adjacent to the nanotube [11–13]. On SiO_2 surfaces, 1 keV is an appropriate acceleration voltage for charging mode. The upper detector of a Hitachi S-4700 SEM was used for detection.

A weakness of SEM is that it cannot clearly distinguish between SWNTs and thin MWNTs, or thin bundles of SWNTs. Thick multiwalled nanotubes (MWNTs) look different from SWNTs in SEM, but SEM alone cannot clearly distinguish between SWNTs and thin MWNTs, such as double walled carbon nanotubes (DWNTs). Only transmission electron microscopy (TEM) images can show directly that nanotubes are single walled. However, Raman and PL spectra of SWNTs are very characteristic and can be used to identify them. Throughout the text we use the terminology "thin nanotubes" to refer to structures identified by SEM which are SWNT candidates, but which have not otherwise been tested or confirmed to be SWNTs. In what follows we use SEM to optimize the yield of these thin nanotubes and then use optical spectroscopy to confirm the existence of SWNTs on samples produced in the optimized process. Transport experiments on single nanotube FETs provide further evidence for a high yield of SWNTs in the optimized process.

3. Results and discussion

Preheating samples in air before the CVD process strongly affects the yield of thin nanotubes. Fig. 3a shows a molybdenum sample grown without such a conditioning step. Fig. 3b shows the same sample type grown after preheating in air for 10 min at 300 °C. Areas of bright contrast are nanotubes imaged by SEM in the charging mode. The CVD process was reduction in hydrogen at 150 sccm and growth in a methane and hydrogen co-flow of 200 sccm and 20 sccm, respectively, at a temperature of 900 °C.

It is likely that the preheat enhances the yield by changing the aluminum sublayer. Early CVD growth experiments used alumina nanoparticles (Al_2O_3) to increase yield by preventing the sintering of catalytic nanoparticles, and allowing for a very high loading of catalyst [2,11]. The use of aluminum as a buffer layer between the substrate and the catalyst particles has also already been shown to
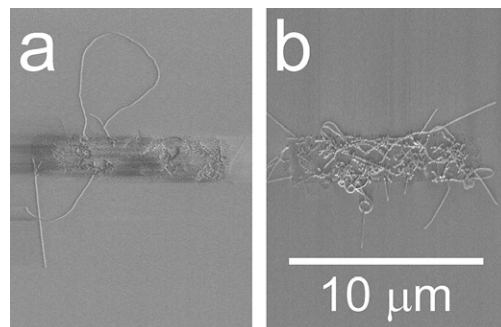
Fig. 4. Effect of iron catalyst film thickness on nanotube yield. Post-growth scanning electron micrographs (1 keV) of catalyst islands with nominally: (a) 1 nm Fe and (b) 2 nm Fe.

have significant effects on the nanotube yield [14–16], and ensuring that it is in the form of alumina is important [16]. The conditioning step should help to more completely oxidize the aluminum. The resulting alumina layer may help prevent catalyst poisoning, and possibly also have a more direct role in catalysis.

Fig. 4 illustrates the effect of varying the iron film thickness on yield. The iron catalyst thin film was nominally 1 nm in (a) and 2 nm in (b), with 1 nm Al sublayers in both cases. This is a catalyst-only sample, as outlined in Fig. 2a. These samples were preheated in air at 300 °C for 10 min, reduced in hydrogen and grown at 900 °C with a methane hydrogen co-flow of 200 sccm and 20 sccm respectively.

Thin nanotubes are visible for both thicknesses. Somewhat lower yield is seen for the 1 nm film. For the 2 nm iron film, there are many thin tubes present, but there are also several thick tubes which are directly resolved in geometrical contrast, even though the magnification is low. These thick curled filaments with micron scale radii of curvature are obviously not SWNTs. At greater film thicknesses, the large, curled filaments predominate, though some thin nanotubes remain. Much thicker films (∼10 nm) yield amorphous, roughly spherical structures with no filamentary character. Thus, the best thickness of iron film to produce reasonable yields of SWNT candidates without excessive growth of material which clearly consists of non-SWNT structures is ∼1 nm or less.

The effect of film thickness seen here is consistent with previous studies. Metal films have been used to catalyze MWNT growth [17], and for the plasma CVD of thick MWNTs the tube diameter scales with film thickness [18]. More recently plasma CVD has been extended to produce SWNTs [19,10]. For thermal CVD of iron films on sapphire, thin films (2 nm) showed larger percentages of SWNTs relative to thick films (5 nm) which produced MWNTs and amorphous carbon [20]. Thin films of 0.5–5 nm in thickness are reported to produce catalyst particles of diameter 5–50 nm when heated to temperatures on the order of 900 °C, and SWNTs were found only to grow by thermal CVD with methane for iron particles between 5 and 15 nm in diameter [21].
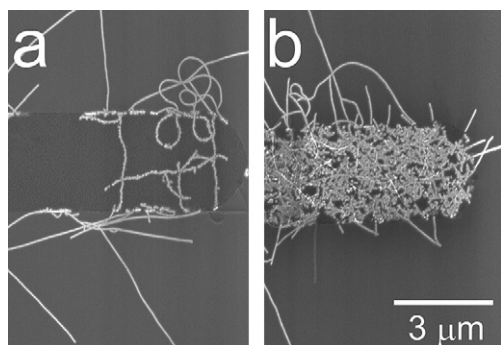

Fig. 3. Effect of preheat conditioning on nanotube yield. Post-growth scanning electron micrographs of catalyst islands (1 keV): (a) no preheat and (b) preheated.
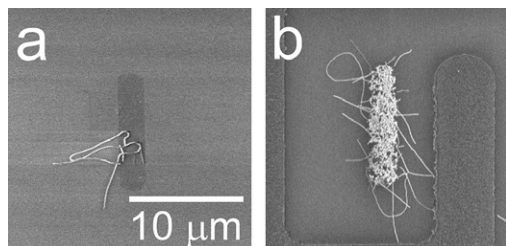
Fig. 5. Effect of molybdenum on nanotube yield. Post-growth scanning electron micrographs (1 keV) of (a) a catalyst island with no molybdenum and (b) a catalyst island surrounded by a molybdenum contact finger.
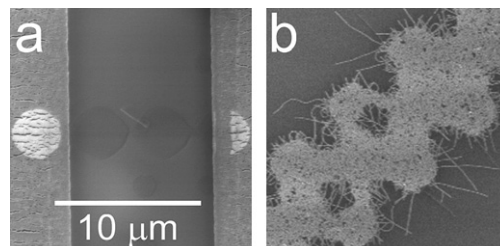

Fig. 6. Effect of temperature on nanotube yield. Scanning electron micrographs (1 keV) of nanotubes grown at (a) 700 °C and (b) 850 °C. Vertical stripes in (a) are molybdenum.

Surprisingly, the presence or absence of molybdenum contact fingers was the dominant factor determining thin nanotube yield. Fig. 5a shows the result of growth on a catalyst-only sample, as outlined in Fig. 2a. Fig. 5b shows a molybdenum contact sample, as outlined in Fig. 2b. Both samples were preheated in air at 300 °C for 10 min, reduced in hydrogen at 900 °C for 10 min and grown at 900 °C in a methane (200 sccm) and hydrogen (20 sccm) co-flow also for 10 min. Without molybdenum just a few thin nanotubes per island were obtained, however, with molybdenum in close proximity the yield was high.

Molybdenum has a catalytic role in combination with iron in methane CVD [22]. A mixture of iron and molybdenum chlorides as a conditioning catalyst upstream from the substrate in hot wall CVD was found to increase yield and length [23]. Iron–molybdenum bimetallic catalysts were found to catalyze nanotube growth at relatively low temperatures [6]. Under certain conditions, the use of molybdenum-alumina conditioning catalyst upstream in a hot wall CVD reactor was found to increase the relative yield of DWNTs [24].

In our case, the molybdenum was spatially separated from the iron catalyst, but it still caused a tremendous increase in thin nanotube yield. The range of the enhancement effect was finite, dropping off as the distance away from the molybdenum patterns increased (at less than ~1 mm away). It is likely that the molybdenum catalyzes the creation of more reactive carbon species from methane, which diffuse to the iron catalyst. It has been reported that benzene could be detected by residual gas analysis of the exhaust in molybdenum enhanced methane CVD [23], however, we found no detectable increase in benzene concentration here.

Molybdenum is used for pre-CVD growth contact fabrication [25]. Pure molybdenum oxidizes readily and the oxide is volatile at CVD growth temperatures. Consistent with Ref. [25], we found that at least some hydrogen co-flow was essential to prevent the molybdenum fingers from eroding.

Growth temperature is another critical variable. The temperature to which the substrate is heated may change the size and shape of the nanoparticles, and if the temperature is too low, particularly in a non-reducing atmosphere, the degree to which nanoparticles are reduced to pure iron may change. To minimize these effects we used a two-step growth process whereby samples were reduced in pure hydrogen at 950 °C and then grown with a methane/hydrogen co-flow with 10–20% hydrogen.

The resulting product showed dramatic changes as a function of temperature. There was high nanotube yield and little notable variation in appearance in the SEM images over the range ~800 °C to ~900 °C. However, below 800 °C the yield dropped. At 700 °C, nanotubes were still present, but it was necessary to search a wide area to find any nanotubes (Fig. 6a). For contrast, a very high yield of nanotubes obtained at 850 °C is shown in Fig. 6b.

These results are consistent with single temperature results using methane but argon in place of hydrogen [26]. This suggests that the drop off in yield over this temperature range has nothing to do with the size of the nanoparticles or their reduced or oxidized state, but simply with the catalytic activity of iron with respect to methane in this range. Since the formation of graphite from methane is spontaneous down to ~650 °C, this is a question of kinetic rate rather than thermodynamic stability. In Ref. [6], Fe/Mo bimetallic catalysts were reported to still have significant nanotube yield for methane CVD at 680 °C, and essentially no yield at 600 °C, which is as expected from the thermodynamic argument.

The temperature dependence of nanotube growth has been reported over a wide range for thermal CVD using acetylene as a precursor. Acetylene decomposes much more readily than methane, and a carbonaceous product is obtained at low temperatures. For CVD with an acetylene burst, using an aluminum buffer layer and Fe/Mo bimetallic thin film catalyst, at 700 °C the yield of nanotubes was poor, with MWNTs tubes appearing at 800 °C and SWNTs appearing by 900 °C [27]. Such thick MWNTs are not generally seen in our case, unless the catalyst layer is too thick, however, the formation of MWNTs is undoubtedly a consequence of the instability of acetylene.

Others working with acetylene, using thin films of iron sputtered directly on silicon, report SWNT formation in the range 850–900 °C with only MWNTs below that [28]. Also, using aluminum thin film and bimetallic Fe/Mo thin film catalyst, and acetylene CVD, MWNTs were reported at temperatures as low as 500 °C, with a mixture of SWNTs and DWNTs formed in the range 800–900 °C
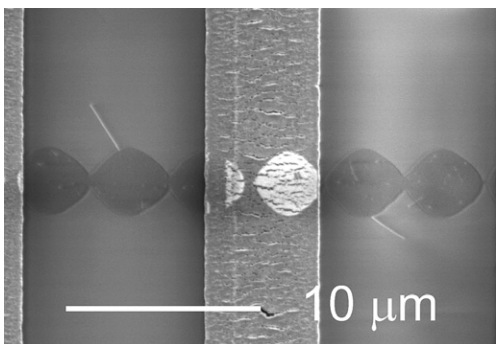
Fig. 7. Nanotube yield at low pressure. Scanning electron micrograph of nanotubes grown at a total pressure of 10 kPa. The vertical stripe is molybdenum, and the circles are catalyst islands.
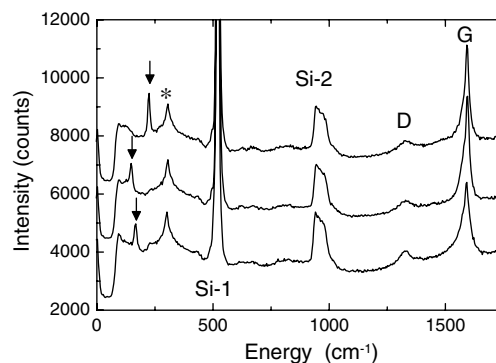

Fig. 8. Raman spectra. Three spectra are shown, offset for clarity. Nanotube related peaks include the radial breathing mode (RBM) labeled with an arrow, and the D and G bands. Substrate related peaks are labeled ∗, Si-1 and Si-2.

[29]. It is interesting that SWNTs form at similar temperature ranges regardless of precursor, and this requires a common mechanism for the nucleation of SWNTs, independent of the hydrocarbon species.

Reducing the gas pressure also caused the thin nanotube yield to fall. The lowest pressure for which we had appreciable growth was a partial pressure of 8 kPa methane, with methane to hydrogen at a 5 to 1 ratio for a total pressure of less than 10 kPa. The reduction step was performed at higher pressure, in case the pressure at this stage had any effect on the size, shape, or state of the catalyst particles. The result is shown in Fig. 7. There is less than one nanotube per catalyst island, and these few nanotubes are fairly short. We even observed a handful of short nanotubes at methane partial pressures of 4.4 kPa (methane to hydrogen ratio of 5 to 1 for a total pressure of ∼5 kPa). However, in that case the yield was extremely low and it was necessary to search over a wide area to find any nanotubes. The drop off in yield at low pressures is similar, but somewhat lower than previously reported for methane thermal CVD [30].

In a vapor–liquid–solid (VLS)-type picture, this drop can be explained. The catalyst particle must remain saturated to precipitate new carbon into the growing nanotube. Desorption is activated with temperature, and for any given temperature carbon will desorb from the catalyst at a given rate. The pressure must be high enough that the adsorption rate can overcome this. As the adsorption rate approaches the desorption rate the growth rate will fall, ceasing when they become equal. It should be noted that the adsorption rate of carbon is lower than the gas impingement rate, by an amount determined by the activity of the catalyst.

We next provide spectroscopic evidence that the thin nanotubes on the high yield samples are indeed single walled. Raman spectra are shown for a high yield (molybdenum) sample in Fig. 8. A home-built confocal micro-Raman setup was used with HeNe (633 nm) laser excitation with 6 mW focused to a ∼5 μm diameter spot. Spectra were taken for nanotubes lying on the surface. Three sample spectra are displayed with a fixed offset for clarity. Radial breathing modes (RBM) are clearly visible and labeled with

an arrow, and are the clear spectroscopic signatures of SWNTs. From top to bottom, RBM frequencies are 224 cm^{-1}, 147 cm^{-1}, and 167 cm^{-1}. A strong G band, and a weaker D band are also visible. Substrate related peaks include the silicon first order (Si-1) and silicon second order (Si-2) peaks as well as a lower energy mode (∗).

A completely independent line of evidence for the formation of SWNTs comes from photoluminescence (PL) spectroscopy. Isolated, suspended SWNTs are strong PL emitters, while tube bundling and interactions with other surfaces quenches PL [31]. To produce such samples, we fabricated arrays of several micron wide trenches and holes by photolithography and reactive ion etching. Subsequent processing was otherwise very similar, with aluminum (1 nm) and iron (1 nm) deposited, and growth at 900 °C with a methane and hydrogen co-flow (2 to 1 ratio). Many holes ended up being bridged by long nanotubes. An example is shown in Fig. 9a. Suspended nanotubes are easily detected by SEM at a range of voltages, and segments on oxide are easily seen at 1 keV via the charging mode. There is actually only a single nanotube in Fig. 9a. It is ∼100 μm in length and coils several times, crossing the hole three times.

Photoluminescence was performed on the same sample, but not at the same position shown in Fig. 9a. A focused
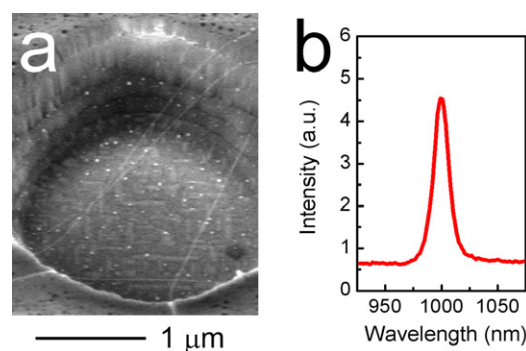

Fig. 9. Suspended nanotubes: (a) scanning electron micrograph of a suspended nanotube and (b) photoluminescence spectrum from a (different) suspended nanotube.

HeNe laser at 633 nm was used for excitation. The luminescence was collected by the same lens, split from the excitation beam by a long pass filter, dispersed by a grating spectrometer, and detected by a liquid nitrogen cooled InGaAs detector. The system was sensitive to luminescence from ∼0.9 μm to ∼1.6 μm. Fig. 9b shows a PL spectrum from a single nanotube. A weak background arises from the luminescence of the underlying substrate. Despite its nanometer scale diameter, the single nanotube PL is much brighter than that from the underlying bulk silicon.

The peak shows the characteristic asymmetric lineshape and narrow linewidth expected from SWNTs suspended in free space [32]. The peak position in this case is consistent with that of an isolated (7,6) nanotube, which is nearly resonant with the 633 nm excitation wavelength, and thus expected to be strong. The detection of PL, along with the characteristic SWNT PL peak shape, and finally the peak position for this excitation wavelength are evidence of SWNT formation.

To test the electrical properties of these nanotubes, we fabricated single nanotube FETs [33]. Catalyst islands were ∼2 μm wide and ranged in length from ∼2 μm to ∼10 μm. Contact fingers were ∼4 μm wide and spaced by ∼6 μm. There was no preferred direction for growth, so we arranged the finger patterns in a spiral pattern around the central catalyst island. The oxide was 1 μm thick, and the doped substrate acted as a backgate. To make a single nanotube transistor, a nanotube had to bridge at least two fingers, meaning that only nanotubes of lengths ∼20 μm or more could be used for devices.

Samples with molybdenum fingers deposited before growth had a device yield ranging from 8% to 20%, with device yield defined as the ratio of patterns with nanotubes bridging at least two contacts to the number of possible devices. Device yield was lower when no molybdenum was used before growth and metal contacts were deposited after CVD (i.e. on top of the nanotubes). In that case the yield ranged from 2% to 16%. The lower yield was a direct consequence of having far fewer nanotubes.

Ironically, at very high nanotube yields the device yield was reduced. For very high nanotube yield, long tubes were less abundant, apparently because most become tangled in the large catalyst area and failed to extend out over the contacts. More speculatively, it is also possible that if the nanotube yield is high, nanotubes compete with their neighbors for reactants, resulting in many shorter nanotubes instead of fewer, longer nanotubes. Our highest device yields came from substrates with molybdenum contacts that were *not* preheated in air, so that the number of nanotubes per catalyst island was lower, but the odds of the tube being long and relatively straight were higher. Many nanotubes were of the order of 100 μm long and so were multiply contacted.

Higher device yields are possible by changing the geometry. For example, most nanotubes were shorter than 20 μm, so many more active devices would be obtained with smaller contact sizes and spacings. Also, larger or dif-
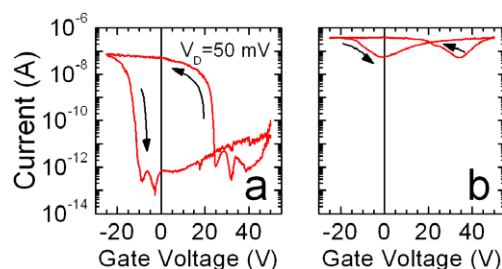

Fig. 10. Single nanotube transistor gate characteristics. Typical gate sweep characteristics for (a) a semiconducting single nanotube transistor and (b) a metallic single nanotube transistor. The direction of the sweep is indicated by the arrows. The source electrode is grounded.

ferently shaped catalyst areas could be used to increase the number of nanotubes. One tradeoff is that if the nanotube yield is too high, the devices will be bridged by multiple nanotubes, and so will not be single nanotube FETs.

Electrical characteristics of the devices were measured in air at room temperature with a commercial probe station. Single nanotube devices, as expected, fell clearly into two classes: semiconductors, which showed a large current modulation with respect to gate voltage, and metals which showed only a mild modulation in current. Fig. 10a shows a gate sweep for a typical semiconducting nanotube. The source electrode is grounded and the voltage on the drain electrode (V_D) is 50 mV. The voltage on the back gate (V_G) was swept over a wide range. Fig. 10b shows a similar sweep for a typical metallic nanotube. The sweeps were highly hysteretic with large gate voltage swings required to "drag" the current back. Hysteresis is commonly seen in nanotube FETs [34] and has been attributed to charging trapped on and in the oxide [35].

These electrical transport experiments provide another line of evidence that at least under optimum conditions, the thin nanotubes are indeed SWNTs. Zone folding theory predicts that single walled nanotubes can be classified as semiconducting or metallic [36]. (More refined theory shows that many of the "metallic" nanotubes actually develop a small bandgap, but the bandgap is sufficiently small that they can be considered metallic here.) The ratio of metallic to semiconducting nanotubes for a random ensemble of individual, isolated SWNTs is expected to be 1/3 to 2/3. Ensembles of MWNTs or bundled SWNTs should deviate strongly from this ratio. Of the devices we measured, ∼65% were semiconducting, consistent with the expectation for single SWNT devices, and inconsistent with expectation for MWNTs and bundles of SWNTs.

4. Summary and conclusion

The cold wall CVD method of nanotube synthesis appears to be just as effective as the standard hot wall method. Given its relative economy, speed and versatility, cold wall CVD could become the preferred method.

High thin nanotube yield can be obtained specifically for thermal cold wall CVD with methane precursors and

iron thin film catalyst with the use of an aluminum thin film sublayer. The thin nanotube yield depends strongly on the presence or absence of molybdenum in proximity to the iron catalyst. Yield is enhanced if a preheating conditioning step is used. The catalyst film must be the right thickness and there are lower bounds to both the pressure and temperature required for nanotube growth. Scanning electron microscopy, Raman spectroscopy, photoluminescence spectroscopy and transport experiments all support the assertion that at least under optimum conditions many, if not all of these are individual, isolated SWNTs. Excessive nanotube yield can reduce device yield, because of tangling, and possibly parasitic growth effects. Consistent yields of nanotubes and nanotube based devices are possible using the methods described here, and some of the future directions to increase FET device yields are clear.

Acknowledgements

References

[1] Pierson HO. Handbook of chemical vapor deposition. Park Ridge, NJ: Noyes; 1992. p. 1–436.

[2] Dai H. Nanotube Growth and Characterization. In: Dresselhaus MS, Dresselhaus G, Avouris Ph, editors. Carbon nanotubes. Top Appl Phys 2001;80:29–53.

[3] Finnie P, Bardwell J, Tsandev I, Tomlinson M, Beaulieu M, Fraser J, et al. Cold wall chemical vapor deposition of single walled carbon nanotubes. J Vac Sci Technol A 2004;22(3):747–51.

[4] Chiashi S, Murakami Y, Miyauchi Y, Maruyama S. Cold wall CVD generation of single-walled carbon nanotubes and in situ Raman scattering measurements of the growth stage. Chem Phys Lett 2004;386(1–3):89–94.

[5] Su M, Li Y, Maynor B, Buldum A, Lu JP, Liu J. Lattice-oriented growth of single-walled carbon nanotubes. J Phys Chem B 2000;104(28):6505–8.

[6] Harutyunyan AR, Pradhan BK, Kim UJ, Chen G, Eklund PC. CVD synthesis of single wall carbon nanotubes under "soft" conditions. Nano Lett 2002;2(5):525–30.

[7] Eres G, Kinkhabwala AA, Cui H, Geohegan DB, Puretzky AA, Lowndes DH. Molecular beam-controlled nucleation and growth of vertically aligned single-wall carbon nanotube arrays. J Phys Chem B 2005;109(35):16684–94.

[8] Jung YJ, Wei B, Vajtai R, Ajayan PM, Homma Y, Prabhakaran K, et al. Mechanism of selective growth of carbon nanotubes on SiO$_2$/Si patterns. Nano Lett 2003;3(4):561–4.

[9] Hata K, Futaba DN, Mizuno K, Namai T, Yumura M, Iijima S. Water assisted highly efficient synthesis of impurity-free single-walled carbon nanotubes. Science 2004;306(5700):1362–4.

[10] Zhong G, Iwasaki T, Honda K, Furukawa Y, Ohdomari I, Kawarada H. Low temperature synthesis of extremely dense and vertically aligned single walled carbon nanotubes. Jpn J Appl Phys 2005;44(4A):1558–61.

[11] Kong J, Soh HT, Cassel AM, Quate CF, Dai H. Synthesis of individual single-walled carbon nanotubes on patterned silicon wafers. Nature 1998;395(6705):878–81.

[12] Brintlinger T, Chen Y-F, Durkop T, Cobas E, Fuhrer MS, Barry JD, et al. Rapid imaging of nanotubes on insulating substrates. Appl Phys Lett 2002;81(13):2454–6.

[13] Homma Y, Suzuki S, Kobayashi Y, Nagase M, Takagi D. Mechanism of bright selective imaging of single-walled carbon nanotubes on insulators by scanning electron microscopy. Appl Phys Lett 2004;84(10):1750–2.

[14] Hongo H, Nihey F, Ichihashi T, Ochiai Y, Yudasaka M, Iijima S. Support materials based on converted aluminum films for chemical vapor deposition growth of single-wall carbon nanotubes. Chem Phys Lett 2003;380(1):158–64.

[15] de los Arcos T, Wu ZM, Oelhafen P. Is aluminum a suitable buffer layer for carbon nanotube growth? Chem Phys Lett 2003;380(3):419–23.

[16] de los Arcos T, Gunnar Garnier M, Oelhafen P, Mathys D, Won Seo J, Domingo C, et al. Strong influence of buffer layer type on carbon nanotube characteristics. Carbon 2004;42(1):187–90.

[17] Ren ZF, Huang ZP, Xu JW, Wang JH, Bush P, Siegal MP, et al. Synthesis of large arrays of well-aligned carbon nanotubes on glass. Science 1998;282(5391):1105–7.

[18] Wei YY, Eres G, Merkulov VI, Lowndes DH. Effect of catalyst film thickness on carbon nanotube growth by selective area chemical vapor deposition. Appl Phys Lett 2001;78(10):1394–6.

[19] Li Y, Mann D, Rolandi M, Kim W, Ural A, Hung S, et al. Preferential growth of semiconducting single-walled carbon nanotubes by a plasma enhanced CVD method. Nano Lett. 2004;4(2):317–21.

[20] Hongo H, Yudasaka M, Ichihashi T, Nihey F, Iijima S. Chemical vapor deposition of single-wall carbon nanotubes on iron-film-coated sapphire substrates. Chem Phys Lett 2002;361(3):349–54.

[21] Takagi D, Homma Y, Kobayashi Y. Selective growth of individual single-walled carbon nanotubes suspended between pillar structures. Physica E 2004;24(1–2):1–5.

[22] Cassell AM, Franklin NR, Tombler TW, Chan EM, Han J, Dai H. Directed growth of free-standing single-walled carbon nanotubes. J Am Chem Soc 1999;121(34):7975–6.

[23] Franklin NR, Dai H. An enhanced CVD approach to extensive nanotube networks with directionality. Adv Mater 2000;12(12):890–4.

[24] Endo M, Huramatsu H, Hayashi T, Kim YA, Terrones M, Dresselhaus MS. Nanotechnology: 'Buckypaper' from coaxial nanotubes. Nature 2005;433(7025):476.

[25] Franklin NR, Wang Q, Tombler TW, Javey A, Shim M, Dai H. Integration of suspended carbon nanotube arrays into electronic devices and electromechanical systems. Appl Phys Lett 2002;81(5):913–5.

[26] Jung YJ, Homma Y, Ogino T, Kobayashi Y, Takagi D, Wei B, et al. High-density, large-area single-walled carbon nanotube networks on nanoscale patterned substrates. J Phys Chem B 2003;107(28):6859–64.

[27] Lacerda RG, Teo KBK, Teh AS, Yang MH, Dalal SH, Jefferson DA, et al. Thin-film metal catalyst for the production of multi-wall and single-wall carbon nanotubes. J Appl Phys 2004;96(8):4456–62.

[28] Nerushev OA, Morjan R-E, Ostrovskii DI, Sveningsson M, Jönsson M, Rohmund F, et al. The temperature dependence of Fe-catalysed growth of carbon nanotubes on silicon substrates. Physica B 2002;323(1–4):51–9.

[29] Cui H, Eres G, Howe JY, Puretkzy A, Varela M, Geohegan DB, et al. Growth behavior of carbon nanotubes on multilayered metal catalyst film in chemical vapor deposition. Chem Phys Lett 2003;374(3–4):222–8.

[30] Homma Y, Yamashita T, Finnie P, Tomita M, Ogino T. Single-walled carbon nanotube growth on silicon substrates using nanoparticle catalysts. Jpn J Appl Phys 2002;41(Part 2,1A/B):L89–91.

[31] Lefebvre J, Homma Y, Finnie P. Bright band gap photoluminescence from unprocessed single-walled carbon nanotubes. Phys Rev Lett 2003;90(21):217401-1–4.

[32] Lefebvre J, Fraser JM, Finnie P, Homma Y. Photoluminescence from an individual single-walled carbon nanotube. Phys Rev B 2004;69(7): 075403-1–075403-5.

[33] Tans SJ, Vershueren ARM, Dekker C. Room-temperature transistor based on a single carbon nanotube. Nature 1998;393(6680):49–52.

[34] Fuhrer MS, Kim BM, Durkop T, Brintlinger T. High-mobility nanotube transistor memory. Nano Lett 2002;2(7):755–9.

[35] Kim W, Javey A, Vermesh O, Wang Q, Li Y, Dai H. Hysteresis caused by water molecules in carbon nanotube field-effect transistors. Nano Lett 2003;3(2):193–8.

[36] Saito R, Dresselhaus G, Dresselhaus MS. Physical properties of carbon nanotubes. London, UK: Imperial College Press; 1998.